
SC-MIL: SPARSELY CODED MULTIPLE INSTANCE LEARNING FOR WHOLE SLIDE IMAGE CLASSIFICATION

Peijie Qiu*, Pan Xiao*

Mallinckrodt Institute of Radiology
Washington University School of Medicine
St. Louis, MO, USA
{peijie.qiu, panxiao}@wsutl.edu

Wenhui Zhu, Yalin Wang

School of Computing and Augmented Intelligence
Arizona State University
Tempe, AZ, USA
{peijie.qiu, panxiao}@wsutl.edu

Aristeidis Sotiras

Mallinckrodt Institute of Radiology
Institute for Informatics, Data Science & Biostatistics
Washington University School of Medicine
St. Louis, MO, USA

ABSTRACT

Multiple Instance Learning (MIL) has been widely used in weakly supervised whole slide image (WSI) classification. Typical MIL methods include a feature embedding part that embeds the instances into features via a pre-trained feature extractor and the MIL aggregator that combines instance embeddings into predictions. The current focus has been directed toward improving these parts by refining the feature embeddings through self-supervised pre-training and modeling the correlations between instances separately. In this paper, we proposed a sparsely coded MIL (SC-MIL) that addresses those two aspects at the same time by leveraging sparse dictionary learning. The sparse dictionary learning captures the similarities of instances by expressing them as a sparse linear combination of atoms in an over-complete dictionary. In addition, imposing sparsity help enhance the instance feature embeddings by suppressing irrelevant instances while retaining the most relevant ones. To make the conventional sparse coding algorithm compatible with deep learning, we unrolled it into an SC module by leveraging deep unrolling. The proposed SC module can be incorporated into any existing MIL framework in a plug-and-play manner with an acceptable computation cost. The experimental results on multiple datasets demonstrated that the proposed SC module could substantially boost the performance of state-of-the-art MIL methods. The codes are available at <https://github.com/sotiraslab/SCMIL.git>.

Keywords Multiple Instance Learning · Weakly Supervised Learning · Whole Slide Imaging · Weakly-Supervised Object Localization · Medical Imaging

1 Introduction

The gigapixel resolution of digital whole slide images (WSIs) enables viewing and analyzing the entire tissue sample in a single image. However, the size and complexity of the images pose significant challenges for pathologists [1]. As a consequence, there is increasing demand for automated workflows to assist WSI analysis. This has propelled the adoption and development of deep learning-based methods in this field [2, 3, 4, 5, 6, 7, 8, 9]. However, applying deep learning methods is challenging due to the enormous size of WSIs and the absence of pixel-level annotations [2]. Weakly-supervised multiple instance learning (MIL) based methods [6, 7, 8, 9] have been proposed to address the aforementioned challenges.

*These two authors contributed equally to this paper

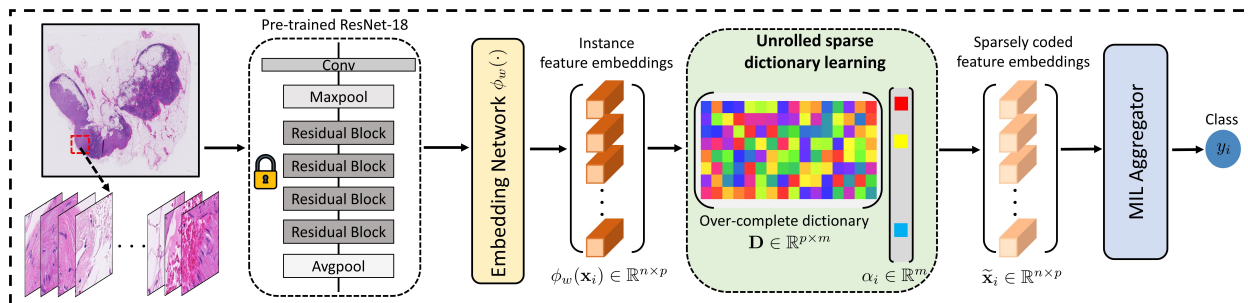


Figure 1: The workflow of the proposed SC-MIL framework in WSI classification. The sparse coding (SC) module conducts end-to-end unrolled sparse dictionary learning and can be easily integrated into any pre-existing Multiple Instance Learning (MIL) framework in a plug-and-play fashion.

In the context of MIL for WSI classification, each WSI is treated as a bag consisting of non-overlapping patches cropped from the WSI slide, with each patch serving as an unlabeled instance. The bag is labeled as positive if at least one of the instances exhibits disease or negative otherwise. A typical way of performing MIL in WSIs adopts a two-stage approach. First, the cropped patches are converted into feature embeddings through a fixed feature extractor. A fixed extractor is preferred over a learned one due to the prohibitively expensive computation for back-propagating with thousands of instances in a bag. Second, a MIL aggregator is applied to combine the local instance feature embeddings to make bag predictions. Such a two-stage learning scheme is potentially suboptimal because the noisy feature embeddings and imbalanced instances (i.e., the positive instances make up only a small portion of all patches in a positive bag) may trap the MIL aggregator into learning an erroneous mapping between embeddings and labels. Besides, the weak supervisory signal hinders the MIL aggregator from capturing correlations between instances [8, 10, 7].

Previous attempts at MIL tackled these two challenges separately. The first class of methods focused on refining the extracted feature embeddings by leveraging self-supervised pretraining [7, 11, 10, 12]. However, these methods require sufficient data and an extra computationally expensive training stage. The second class of methods focused on improving the MIL aggregator, so that it can better capture cross-instance correlations, while imposing sparsity constraints on the local instance attention (e.g., selecting k most important instances) to discard negative instances [13, 14, 7, 9]. However, these two classes of methods are strongly interrelated as better instance feature embeddings that are sparse and capable of modeling the invariance of the same type of biological tissues would also simplify the task of the MIL aggregator. In addition, the sparse feature embeddings are a low-dimensional representation of the initial instance embeddings from the feature extractor, which is shown empirically to be beneficial to WSI representation as the high-dimensional WSI representation lies in a low-dimensional manifold [10, 12].

Sparse dictionary learning offers a natural way to impose sparsity in instance feature embeddings and can model the similarities of instances from the same tissue type through an over-complete dictionary. In light of this, we proposed a novel MIL framework termed sparsely coded MIL (SC-MIL), which performs sparse dictionary learning on the initial feature embeddings. However, the conventional algorithms for sparse dictionary learning are not directly compatible with deep neural networks and require extensive hyperparameter tuning. Inspired by [15], we designed an unrolled SC module for sparse dictionary learning that can be optimized through end-to-end learning. The proposed SC module is orthogonal to existing MIL frameworks and can be easily integrated into them in a plug-and-play fashion with acceptable additional computation. The experimental results on multiple datasets and various tasks demonstrated the effectiveness of the proposed method in boosting the performance of state-of-the-art MIL methods.

2 Related Work

2.1 MIL in WSI classification

MIL methods can be broadly divided into two major categories: instance-level MIL and bag-level MIL. Typically, the instance-level methods [16, 17, 18, 19, 20] start with training a network to predict instance-level labels that are assigned by propagating the bag-level label to each of its instances. They aggregate the predicted instance-level labels to obtain the corresponding bag-level label afterward. However, due to the fact that only a small fraction of positive instances in a bag are associated with a disease in WSIs, the negative instances in a positive bag are often mislabeled. Despite numerous attempts to purify the instance-level labels, empirical studies have consistently shown that instance-level methods exhibit inferior performance compared to their bag-level counterparts [8, 21].

Bag-level MIL methods [6, 7, 8, 9, 21, 13, 22, 23, 11, 10, 12, 14] follow a two-stage learning process: they first embed the instances into feature representation using a pre-trained feature extractor and then perform MIL aggregation to generate bag-level predictions. Previous explorations in bag-level MIL primarily focused on two directions. The first direction is to enhance the MIL aggregator. Following this direction of work, the attention-based MIL [6, 13] turned the traditional non-parametric poolings, e.g., max/mean-pooling [21], into trainable ones through an attention mechanism. However, initial attempts treated each instance independently without considering their similarities. Many follow-up works addressed this limitation by leveraging graph convolutional networks [14], non-local attention [7], transformer [8], and knowledge distillation [9]. The second direction is to improve the feature embedding by mainly leveraging self-supervised pre-training [7, 11, 10, 12]. However, these methods need a sufficient amount of data for task-specific training and are computationally expensive.

Our work is closely related to [10], which enhanced the feature embedding through a low-rank guided self-supervised pre-training and improved the attention-based MIL aggregator to harness low-rank property. However, it still requires an extra self-supervised training stage and is tailored to a specific MIL aggregator. In contrast, our work can achieve both feature enhancement and model global instance similarities by a single module, as well as can be incorporated into current MIL methods in a plug-and-play fashion.

2.2 Sparse Dictionary Learning and Algorithm Unrolling

Sparse dictionary learning is widely used in the realm of machine learning and signal processing, with applications in image restoration [24, 25, 26, 27], image classification [28], and compressed sensing [29]. Its objective is to obtain a compact and robust representation of data through a sparse linear combination of atoms in a dictionary that can effectively approximate the input signal [24, 30]. This process is formulated as an optimization problem solved by iterative algorithms such as K-SVD [31], ISTA [32], FISTA [33], and Coordinate Descent [34]. However, these iterative algorithms are not directly compatible with deep neural networks for end-to-end training. Additionally, the convergence of the iterative algorithms is highly sensitive to the choice of hyperparameters, e.g., stepsize. The algorithm unrolling [15, 26], motivated by [35], addressed these problems by reformulating sparse coding as layers in network architectures that can be directly optimized through back-propagation. In this work, we considered the unrolled version of ISTA for sparse dictionary learning, which is closely related to (but not the same as) the one used in [15, 26].

3 Method

The proposed method performed the unrolled sparse dictionary learning on the instance embeddings to enhance feature embeddings and model global similarities between instances, as depicted in Fig. 1.

Problem Formulation. Without loss of generality, let us consider the problem of bag-level binary MIL classification. Its objective is to learn a mapping from a set of bags $\{\mathbf{x}_1, \mathbf{x}_2, \dots, \mathbf{x}_b\}$ to corresponding labels $\{z_1, z_2, \dots, z_b\}$, where each bag \mathbf{x}_i contains n instances $\{x_{i,1}, x_{i,2}, \dots, x_{i,n}\}$ with $x_{i,j} \in \mathbb{R}^p$, where p denotes the dimension of each instance. Mathematically, the bag-level binary MIL classification is defined as:

$$y_i = \begin{cases} 0, & \text{iff } \sum_{j=1}^n y_{i,j} = 0 \\ 1, & \text{otherwise,} \end{cases} \quad (1)$$

where $y_{i,j} \in \{0, 1\}$ denotes the unknown instance-level label of the i -th bag, and n can vary from bag to bag. A MIL aggregator combines the instance-level predictions within a bag to produce a bag-level prediction:

$$\hat{y}_i = f_{cls}(\sigma(\{\phi_w(x_{i,1}), \phi_w(x_{i,2}), \dots, \phi_w(x_{i,n})\})), \quad (2)$$

where $f_{cls}(\cdot)$ refers to a bag-level classifier, ϕ_w denotes an embedding network parameterized by w that operates on the instance level, and σ is a permutation-invariant function. The σ is also known as the MIL pooling operation. We consider four popular MIL pooling methods (i.e., attention-based [6], non-local-based [7], transformer-based [8], and knowledge distillation-based [9]) in this work.

3.1 Sparsely Coded MIL

The low-dimensional representation of instance embeddings is empirically shown to effectively improve WSI representation [10, 12]. We consider there exists a low-dimensional representation of initial instance embeddings $\phi_w(\mathbf{x}_i)$ that can be expressed as a linear combination of $s \ll m$ atoms from an over-complete dictionary $\mathbf{D} \in \mathbb{R}^{p \times m}$, where m is referred to as the number of atoms in a dictionary. The sparsely coded feature embeddings can be expressed as

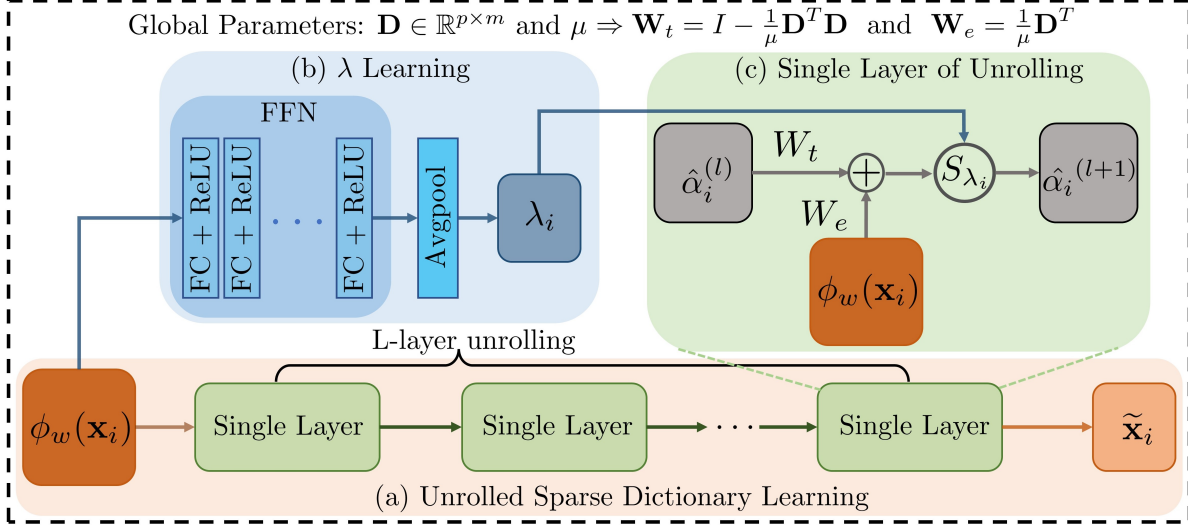


Figure 2: The proposed SC module: (a) The unrolled ISTA learning scheme of the sparse dictionary learning (b) the λ learning block which is implemented as a feed-forward network followed by an average pooling. (c) A single network layer of the unrolling network for sparse dictionary learning.

$\tilde{\mathbf{x}}_i = \mathbf{D}\alpha_i$, where $\alpha_i \in \mathbb{R}^m$ denotes the sparse coefficients for each instance embeddings $\phi_w(\mathbf{x}_i)$. This process can be formally defined as sparse dictionary learning, which can be formulated as an optimization problem:

$$\hat{\alpha}_i = \arg \min_{\alpha_i} \frac{1}{2} \|\mathbf{D}\alpha_i - \phi_w(\mathbf{x}_i)\|_2^2 + \lambda \|\alpha_i\|_1, \lambda > 0 \quad (3)$$

where λ controls the strength of the sparsity regularization. The ℓ_1 penalty of the α_i is an approximate relaxation of the ℓ_0 sparsity, which results in a convex optimization. An effective solver of Eqn. 3 is the Iterative Soft Thresholding Algorithm (ISTA) [32], which is given as a proximal update

$$\hat{\alpha}_i^{(t+1)} = S_\lambda \left(\hat{\alpha}_i^{(t)} - \frac{1}{\mu} \mathbf{D}^T (\mathbf{D}\hat{\alpha}_i^{(t)} - \phi_w(\mathbf{x}_i)) \right), \hat{\alpha}_i^{(0)} = 0 \quad (4)$$

where μ is the stepsize, and t denotes t -th iteration. $S_\lambda(\cdot)$ is the element-wise soft-thresholding operator, serving as the proximal projection

$$[S_\lambda(\mathbf{v})]_j = \text{sign}(v_j) \cdot \max\{|v_j| - \lambda, 0\}, \quad (5)$$

where v_j is the j -th element of \mathbf{v} , and $\max\{\cdot\}$ is the element-wise max operator.

3.2 Unrolled Sparse Dictionary Learning

Even though the ISTA can be guaranteed to converge to a global optimum, its convergence requires a proper choice of stepsize μ and regularization strength λ . Furthermore, the dictionary should be optimized for a specific task given the input dataset. The proximal update enables unrolling the ISTA-based sparse dictionary learning into a fully trainable scheme. The reparameterization of Eqn. 3

$$\hat{\alpha}_i^{(t+1)} = S_\lambda \left(\mathbf{W}_t \hat{\alpha}_i^{(t)} + \mathbf{W}_e \phi_w(\mathbf{x}_i) \right) \text{ with} \quad (6)$$

$$\mathbf{W}_t = I - \frac{1}{\mu} \mathbf{D}^T \mathbf{D} \text{ and } \mathbf{W}_e = \frac{1}{\mu} \mathbf{D}^T$$

yields the learnable ISTA (LISTA) that can optimize the parameters (i.e., \mathbf{D} , μ , and λ) in a trainable fashion. Given the dictionary \mathbf{D} , stepsize μ , and sparsity strength λ , the update rule in Eqn. 6 can be recast into a single network layer, as depicted in Fig. 2(c). The cascaded repeat of such single network layer L times results in an L -layer unrolled network for sparse dictionary learning (see Fig. 2(a)), while maintaining the same computational path in the Eqn. 3. This is also equivalent to performing L iterations of LISTA update in Eqn. 6. As a result, we unrolled the ISTA-based sparse dictionary learning into a single module called the SC module. The number of unrolled layers L is a hyperparameter that can be tuned to balance the trade-off between model complexity and performance.

Learning the over-complete dictionary. The over-complete dictionary \mathbf{D} in the sparse dictionary learning can be used to model the similarities across instances, which is a crucial feature in MIL. To further achieve a globally invariant instance representation belonging to the same tissue type, we set the dictionary \mathbf{D} as a global parameter that is optimized for all bags. As each operation (i.e., matrix multiplication, summation, soft-thresholding) in a single unrolling layer is differentiable, the optimization of \mathbf{D} can be achieved by backpropagation via training the binary MIL classification task in an end-to-end fashion. To speed up its convergence, the dictionary is initialized with an over-complete discrete cosine transform matrix [36].

Learning the optimal λ . The sparsity regularization strength λ is an important parameter to select in the vanilla ISTA update in Eqn. 3. The value of λ determines a trade-off between the sparsity and expressiveness of the sparse dictionary learning and therefore requires careful tuning. However, in the context of SC-MIL, the optimal choice of λ can vary from bag to bag, making it prohibitively difficult to be tuned manually. To this end, we formulated the evaluation of the optimal λ_i for each bag as a regression task, inspired by [15]. Specifically, λ_i was parameterized as a simple feed-forward network (FFN) $f_\theta(\phi_w(\mathbf{x}_i))$ (see Fig. 2(b)), where θ denotes the network’s parameters. In this work, the FFN consisted of three fully-connected layers, with ReLU activation applied to each. An average pooling layer was added after the FFN to produce a scalar output for λ_i . We chose average pooling because each target instance embedding in a bag contributes equally to the sparsity.

Learning the optimal stepsize μ . The choice of stepsize μ is a key factor in the convergence of the vanilla ISTA. One commonly used and effective choice is to set μ as the square of the spectral norm of the dictionary. Nonetheless, the optimal stepsize is prone to vary across different datasets and tasks. To determine the optimal stepsize μ for a given dataset, we made it learnable by setting it as a global parameter initialized with the square of the spectral norm of the dictionary.

4 Experiments and Results

4.1 Dataset and Feature Extraction

We conducted various experiments on multiple datasets, including five classical MIL benchmarks, the MNIST-bags dataset [6], the CAMELYON16 dataset [37], and the Cancer Genome Atlas non-small cell lung cancer (TCGA-NSCLC) dataset to validate the effectiveness of the proposed method.

Classical MIL benchmarks. The five classical MIL benchmark datasets consist of MUSK1, MUSK2, FOX, TIGER, and ELEPHANT dataset. The MUSK1 and MUSK2 datasets are used to predict the impacts of drugs given the molecule conformations. Each bag consists of several conformations of the same molecule. The label for the bag is positive if at least one of its conformations has the desired drug effect and negative if none is effective [38]. The FOX, TIGER, and ELEPHANT datasets identify if the target animal is presented in a bag. Each bag consists of a set of features extracted from segments of an image. Positive bags refer to images that contain the animals of interest, whereas negative bags are images where no such animal is present [39].

MNIST-bags dataset. The MNIST-bags dataset [6] consists of bags made up of a random number of grayscale handwritten digits (instances) from the MNIST dataset. Following [6], the digit of interest was designated as ‘9’, and any bag containing at least one instance of ‘9’ was labeled as positive. The average number of instances per bag was set to ten, with a standard deviation of two. We used this dataset for explanations after incorporating the proposed SC module into attention-based MIL [6].

CAMELYON16 dataset. The CAMELYON16 is a publicly available WSI dataset for detecting metastatic breast cancer in lymph node tissue. The dataset consists of 399 WSIs (one corrupted sample was discarded) of lymph node tissue, officially split into a training set of 270 samples and a testing set of 129 samples. Each WSI is accompanied by a binary label, annotated by pathologists, indicating the presence or absence of metastatic cancer in the lymph node tissue. The dataset also includes detailed annotations of the regions of interest within each WSI that contains cancerous tissue. By following the preprocessing procedures outlined in [7], we cropped the WSIs into non-over-lapping patches of size 224×224 . This resulted in a total of around 3.37 million patches at $\times 20$ magnification, with an average of 8451 patches per bag.

TCGA-NSCLC dataset. The TCGA-NSCLC is a different WSI dataset that is used for identifying two sub-types of lung cancer: lung squamous cell carcinoma and lung adenocarcinoma. Following [7], we divided a total of 1037 diagnostic WSIs into a training set of 744, a validation set of 83, and a testing set of 210 WSIs. After performing the identical preprocessing applied to the CAMELYON16 dataset, roughly 10.30 million patches were extracted at a $\times 20$ magnification level. On average, each bag consisted of 10355 patches.

Table 1: Performance comparison on five classical MIL benchmark datasets. Each experiment was performed five times with 10-fold cross-validation. We reported the mean of the classification accuracy (\pm the standard deviation of the mean). Previous benchmark results were obtained from [6, 7] under the same experimental settings. The best performance is marked in bold, while the second performance is underlined.

Methods	MUSK1	MUSK2	FOX	TIGER	ELEPHANT
mi-Net [21]	0.889 \pm 0.039	0.858 \pm 0.049	0.613 \pm 0.035	0.824 \pm 0.034	0.858 \pm 0.037
MI-Net [21]	0.887 \pm 0.041	0.859 \pm 0.046	0.622 \pm 0.038	0.830 \pm 0.032	0.862 \pm 0.034
MI-Net with DS [21]	0.894 \pm 0.042	0.874 \pm 0.043	0.630 \pm 0.037	0.845 \pm 0.039	0.872 \pm 0.032
MI-Net with RC [21]	0.898 \pm 0.043	0.873 \pm 0.044	0.619 \pm 0.047	0.836 \pm 0.037	0.857 \pm 0.040
ABMIL [6]	0.892 \pm 0.040	0.858 \pm 0.048	0.615 \pm 0.043	0.839 \pm 0.022	0.868 \pm 0.022
ABMIL-Gated [6]	0.900 \pm 0.050	0.863 \pm 0.042	0.603 \pm 0.029	0.845 \pm 0.018	0.857 \pm 0.027
GNN-MIL [43]	0.917 \pm 0.048	0.892 \pm 0.011	0.679 \pm 0.007	0.876 \pm 0.015	0.903 \pm 0.010
DP-MINN [44]	0.907 \pm 0.036	0.926 \pm 0.043	0.655 \pm 0.052	0.897 \pm 0.028	0.894 \pm 0.030
NLMIL [45]	0.921 \pm 0.017	0.910 \pm 0.009	0.703 \pm 0.035	0.857 \pm 0.013	0.876 \pm 0.011
ANLMIL [46]	0.912 \pm 0.009	0.822 \pm 0.084	0.643 \pm 0.012	0.733 \pm 0.068	0.883 \pm 0.014
DSMIL [7]	0.932 \pm 0.023	0.930 \pm 0.020	0.729 \pm 0.018	0.869 \pm 0.008	0.925 \pm 0.007
ABMIL w/ SC	<u>0.958 \pm 0.015</u>	<u>0.958 \pm 0.008</u>	<u>0.789 \pm 0.015</u>	<u>0.933 \pm 0.007</u>	<u>0.949 \pm 0.004</u>
ABMIL-Gated w/ SC	0.969 \pm 0.004	0.960 \pm 0.008	0.791 \pm 0.007	0.948 \pm 0.004	0.956 \pm 0.004

Feature Extractor. The five classical MIL benchmarks comprise pre-extracted feature vectors of instances. A simple FFN with the same architecture as in [21, 6] was deployed for further feature embedding. In the case of the MNIST-bags dataset, we employed the identical feature extractor (i.e., LeNet5 [40]) and instance-level embedding network as those used in [6]. We adopted the ResNet-18 [41] as the feature extractor for WSI classification by removing the last fully-connected layer (see Fig. 1). After passing through the feature extractor, each patch in WSIs is embedded into a 512-dimensional vector. We evaluated two distinct pre-training techniques. The first one involved pre-training ResNet-18 on the ImageNet, which is released by PyTorch. Given the effectiveness of self-supervised pre-training, we adapted contrastive learning as the second pre-training method. Following the same experimental settings of [7], we pre-trained the feature extractor on the training set of CAMELYON16 and TCGA-NSCLC, separately, using the SimCLR framework [42].

4.2 Experiments

Baseline. For the classical MIL benchmark datasets, we compared the proposed method to a series of deep learning-based MIL methods, including mi-Net and MI-Net [21], ABMIL and ABMIL-Gated [6], GNN-MIL [43], DP-MINN [44], and three non-local MIL pooling methods (i.e., NLMIL [45], ANLMIL [46], and DSMIL [7]). In the case of WSI classification, we considered plugging the proposed SC module into four different types of MIL aggregators, i.e., ABMIL with gated attention [6], DSMIL [7], TransMIL [8] and DTFD-MIL with maximum attention score selection (MaxS) [9].

Experiment setup and evaluation metrics. In this study, distinct experimental procedures were employed for different datasets. Specifically, for the classical MIL datasets, we performed 10-fold cross-validation on each dataset with five repetitions per experiment, using classification accuracy as the primary metric. To validate the effectiveness of the proposed method, we incorporated the proposed SC module into the ABMIL framework using two distinct attention mechanisms, denoted by ABMIL w/ SC and ABMIL-Gated w/ SC. Additionally, 200 bags were used for training, and 50 bags were employed for testing in the MNIST-bags dataset. For the two WSIs datasets, we utilized the aforementioned training and testing partitions. We conducted experiments on features extracted from those above two differently pre-trained ResNet-18. The evaluation metrics used were the classification accuracy and the area under the receiver operating characteristic curve (AUC) scores.

Implementation details. The cross-entropy loss was adopted to train all the models in this work. In all results reported in Tables 1 and 2, the number of atoms in a dictionary was set to $m = 16$, and the number of unrolled layers was set to $L = 6$. The batch size was set to 1 for all the experiments. The models on classic MIL datasets were trained using an Adam optimizer for 40 epochs with initial learning of 1×10^{-4} and ℓ_2 weight decay of 5×10^{-3} . The initial learning rate was adjusted through a cosine annealing scheduler. In the cases of the MNIST-bags dataset, we used the same settings for training but with a different initial learning rate of 5×10^{-4} and a weight decay of 1×10^{-4} . In the WSI classification tasks, we trained all four MIL aggregators for 200 epochs by following the default training settings in

Table 2: Comparisons to state-of-the-art methods on the CAMELYON16 and TCGA-NSCLC datasets. The classification accuracy (%) and AUC (%) were reported. The +SC denotes incorporating the proposed SC module into the corresponding MIL methods, and Δ denotes the performance gain.

Methods			CAMELYON16		TCGA-NSCLC		
			Accuracy	AUC	Accuracy	AUC	
ResNet-18 ImageNet Pretrained	ABMIL-Gated		80.62	80.89	82.86	91.02	
		+SC Δ	82.17 +1.55	84.12 +3.23	89.05 +6.19	94.03 +3.01	
	DSMIL		82.17	85.04	77.62	89.36	
		+SC Δ	84.50 +2.33	86.09 +1.05	86.67 +9.05	94.14 +4.78	
	TransMIL		80.62	81.86	84.76	92.00	
		+SC Δ	82.17 +1.55	87.68 +5.82	86.67 +1.91	94.43 +2.43	
	DTFD-MIL (MaxS)		82.95	86.07	83.33	90.25	
		+SC Δ	85.27 +2.32	86.44 +0.37	87.62 +4.29	93.96 +3.71	
	ResNet-18 SimCLR Pretrained	ABMIL-Gated		86.05	86.30	85.71	93.27
			+SC Δ	89.15 +3.10	90.41 +4.11	88.57 +2.86	95.28 +2.01
DSMIL			86.82	85.76	86.67	93.15	
		+SC Δ	88.37 +1.55	87.53 +1.77	90.48 +3.81	95.26 +2.11	
TransMIL			86.05	90.97	88.57	95.82	
		+SC Δ	90.70 +4.65	91.18 +0.21	91.43 +2.86	96.29 +0.47	
DTFD-MIL (MaxS)			82.95	89.54	84.29	90.37	
		+SC Δ	86.05 +3.10	92.55 +3.01	88.57 +4.28	94.20 +3.83	

their official implementations [6, 7, 8, 9]. All experiments were performed on four Nvidia Tesla V100 GPUs, each with 32G of memory.

4.3 Results on classic MIL benchmarks

After plugging the proposed SC module, the ABMIL w/ SC and ABMIL-Gated w/ SC outperformed the previous state-of-the-art methods across all five MIL benchmark datasets regarding classification accuracy (see Table 1). The ABMIL-Gated w/ SC achieved the best performance by improving the previous state-of-the-art accuracy by an average of 4.95%, with 3.97% on MUSK1, 3.23% on MUSK2, 8.50% on FOX, 5.69% on TIGER, and 3.35% on ELEPHANT. In addition, the ABMIL-Gated w/ SC exhibited the highest stability with an average standard deviation of 0.0054 in accuracy.

4.4 Results on WSI classification

The performance of the four different types of MIL aggregators using two distinct pre-training methods was consistently boosted by integrating the proposed SC module (see Table 2). This indicates that the performance gain of the proposed SC module is agnostic to different MIL aggregators and pre-training methods. On the CAMELYON16 dataset, plugging in the proposed SC module resulted in an average AUC gain of 4.01% and 2.60% using ImageNet pre-training and SimCLR pre-training, respectively. Similarly, there was an average accuracy improvement of 2.37% and 3.63% when applying the SC module on two distinctly pre-trained feature embeddings. On the TCGA-NSCLC dataset, we observed an average increase of 3.69% and 2.28% in AUC using ImageNet pre-training and SimCLR pre-training, respectively. An average improvement of 6.63% and 4.01% in accuracy was observed using features obtained from the aforementioned two differently pre-trained ResNet-18. .

Table 3: Ablation studies on different parameter selections in the proposed SC module. The FLOPs were measured based on a bag containing 120 instances.

# Atoms (m)	# Params	FLOPs	AUC
$m = 4$	73.81K	10.02K	88.93
$m = 8$	94.04K	18.59K	89.52
$m = 16$	189.97K	86.13K	90.41
$m = 32$	561.68K	888.60K	90.70

# Layers (L)	FLOPs	AUC
$L = 2$	53.93K	90.10
$L = 4$	70.03K	89.91
$L = 6$	86.13K	90.41
$L = 8$	102.22K	91.08

 (a) The number of atoms in a dictionary when $L = 6$

 (b) The number of unrolled layers when $m = 16$

Our findings also indicated that the improvement in ImageNet pre-training (an average of 3.85% in AUC and 4.50% in accuracy) was larger than SimCLR pre-training (2.44% in AUC and 3.82% in accuracy). This suggests that enhancing high-quality feature embedding (e.g., SimCLR pre-training) is more challenging than a low-quality one (e.g., ImageNet pre-training), and better feature embedding generally leads to better performance. Importantly, the performance improvement gained from the proposed SC module (an average of 3.85% in AUC and 4.50% in accuracy) was comparable to that of the SimCLR pre-training (4.21% in AUC and 4.98% in accuracy). Nonetheless, different from self-supervised pre-training, integrating the proposed SC module into current MIL frameworks can be achieved in a plug-and-play fashion without the need for a separate training stage.

4.5 Ablation Studies

To investigate the impact of hyperparameter selection (i.e., number of atoms in the dictionary m and number of unrolled layers L) on performance, we conducted a series of ablation studies on the SC module. Using SimCLR pre-trained features on the CAMELYON16 dataset, the ABMIL-Gated was employed to carry out the ablation studies. To examine the impact of the number of atoms, we maintained the number of unrolled layers at 6. We observed that increasing the number of atoms resulted in a gradual improvement in performance as well as an increase in parameters and computation (Table 3a). We noticed that increasing the number of atoms from 16 to 32 resulted in a minor performance gain (0.32% in AUC), while the computation rose by around ten times. To investigate the effect of the number of unrolled layers on the performance, we fixed the number of atoms at 16. Overall, increasing the number of unrolled layers progressively led to an improvement in AUC, but at the expense of increased computation (Table 3b). A drop was observed when increasing L from 2 to 4, which may be attributed to minor fluctuation in the convergence path of LISTA.

4.6 Interpretability

The proposed SC module not only improved the performance of various MIL aggregators but also enhanced interpretability. On the MNIST-bags dataset, the vanilla ABMIL exhibited an uneven distribution of attention scores (0.1780 ± 0.0748) for the target digit '9', which was attributed to its unawareness of cross-instance correlations (Fig. 3(a)). After incorporating the proposed SC module, the ABMIL w/ SC exhibited more evenly distributed attention scores (0.1995 ± 0.0341) (Fig. 3(b)). Comparable findings were observed in the localization of the morphology within the

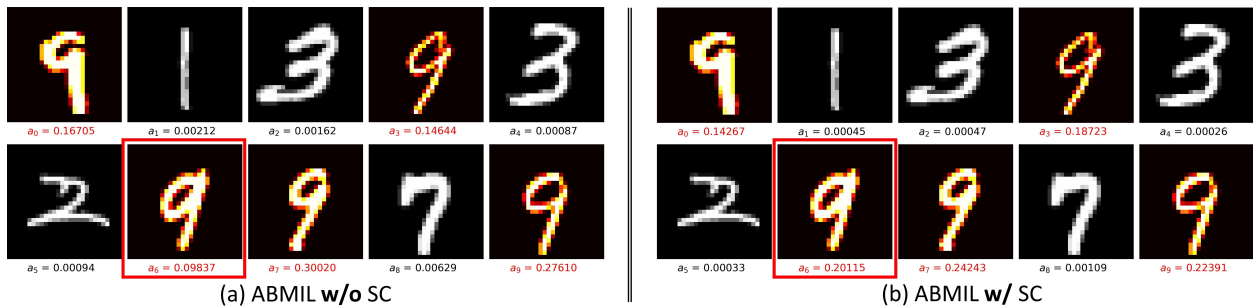


Figure 3: Comparison of attention weights for a positive bag on the MNIST-bags dataset obtained from (a) ABMIL w/o SC module and (b) ABMIL w/ SC module. In the vanilla ABMIL, the positive instance with a low attention weight was highlighted by the red box, whereas in the ABMIL w/ SC, the same highlighted positive instance had a higher attention weight.

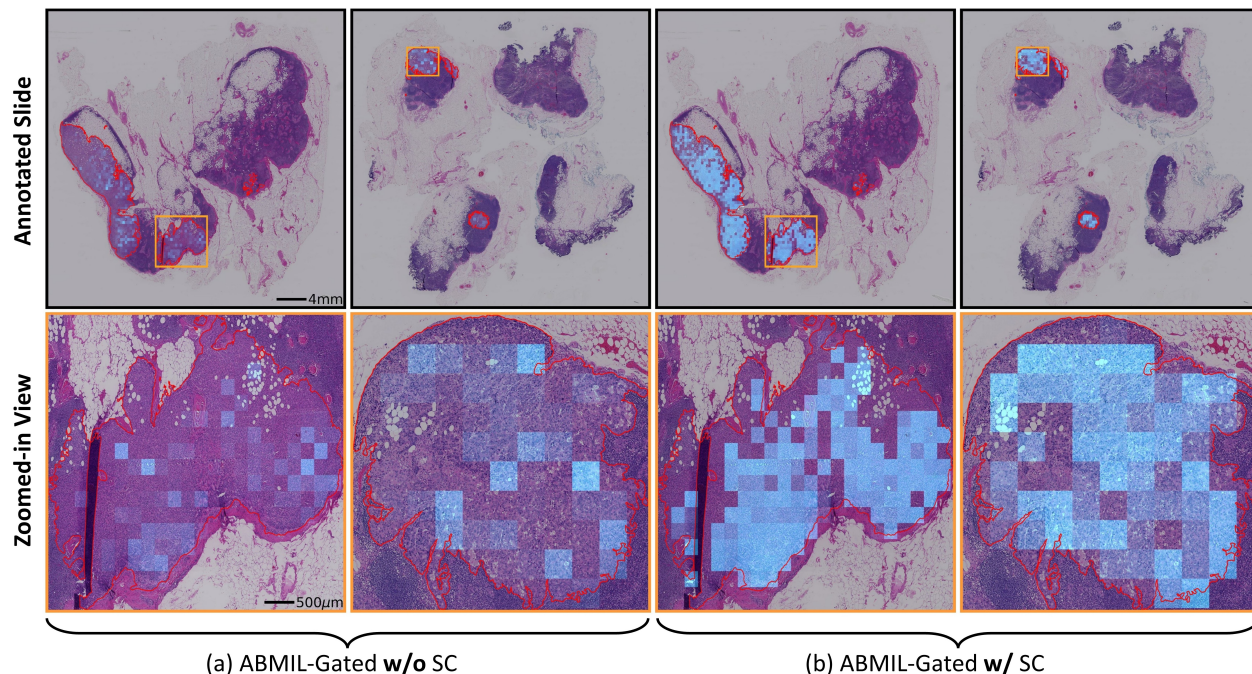


Figure 4: The tumor localization in CAMELYON16 using the SimCLR pre-trained features: (a) the attention map from ABMIL-Gated **w/o** SC and (b) the attention map from ABMIL-Gated **w/** SC.

region of interest in WSIs. The attention scores were employed to gauge the significance of each patch, providing insights into important morphology that can guide clinical diagnosis. Specifically, the vanilla ABMIL-Gated exhibited poor tumor localization on the CAMELYON16 dataset (see Fig. 4(a)), missing most of the tumor patches. However, the integration of the SC module significantly enhanced the localization performance of the ABMIL-Gated (see Fig. 4(b)), aligning well with the annotated tumor morphology. The findings from both the MNIST-bags dataset and the WSI dataset evidenced that the global dictionary of instance embeddings in the proposed SC module can effectively capture cross-instance similarities, leading to enhanced localization performance.

5 Conclusion

In this paper, we proposed a novel MIL framework, termed SC-MIL, by leveraging unrolled sparse dictionary learning. The proposed method simultaneously enhances the instance feature embedding and models cross-instance similarities without a huge computational burden. Importantly, experimental results from multiple benchmarks across various tasks showed that the performance of state-of-the-art MIL methods could be further boosted by incorporating the proposed SC module in a plug-and-play manner. The proposed method exhibits great potential to be used in real-world applications to aid in drug effect prediction, diabetic retinopathy grading, and the diagnosis and pathological analysis of cancers using histology. The proposed method is particularly effective in real scenarios where the self-supervised pre-training for the enhancement of feature embedding is infeasible due to the limited data size.

Limitations. Although the unrolled sparse dictionary learning can automatically handle expensive hyperparameter tuning in traditional iterative solutions, a limitation of the proposed method is that it still necessitates minor hyperparameter tuning, e.g., the number of atoms and learning rate. In addition, plugging the SC module into existing MIL frameworks may result in a slight slowdown in convergence. We will explore these limitations in future work.

References

- [1] Lei He, L Rodney Long, Sameer Antani, and George R Thoma. Histology image analysis for carcinoma detection and grading. *Computer methods and programs in biomedicine*, 107(3):538–556, 2012.
- [2] Geert Litjens, Clara I Sánchez, Nadya Timofeeva, Meyke Hermsen, Iris Nagtegaal, Iringo Kovacs, Christina Hulsbergen-Van De Kaa, Peter Bult, Bram Van Ginneken, and Jeroen Van Der Laak. Deep learning as a tool for increased accuracy and efficiency of histopathological diagnosis. *Scientific reports*, 6(1):1–11, 2016.

- [3] Xiaomin Zhou, Chen Li, Md Mamunur Rahaman, Yudong Yao, Shiliang Ai, Changhao Sun, Qian Wang, Yong Zhang, Mo Li, Xiaoyan Li, et al. A comprehensive review for breast histopathology image analysis using classical and deep neural networks. *IEEE Access*, 8:90931–90956, 2020.
- [4] Jakob Nikolas Kather, Alexander T Pearson, Niels Halama, Dirk Jäger, Jeremias Krause, Sven H Loosen, Alexander Marx, Peter Boor, Frank Tacke, Ulf Peter Neumann, et al. Deep learning can predict microsatellite instability directly from histology in gastrointestinal cancer. *Nature medicine*, 25(7):1054–1056, 2019.
- [5] Nicolas Coudray, Paolo Santiago Ocampo, Theodore Sakellaropoulos, Navneet Narula, Matija Snuderl, David Fenyö, Andre L Moreira, Narges Razavian, and Aristotelis Tsirigos. Classification and mutation prediction from non-small cell lung cancer histopathology images using deep learning. *Nature medicine*, 24(10):1559–1567, 2018.
- [6] Maximilian Ilse, Jakub Tomczak, and Max Welling. Attention-based deep multiple instance learning. In *International conference on machine learning*, pages 2127–2136. PMLR, 2018.
- [7] Bin Li, Yin Li, and Kevin W Eliceiri. Dual-stream multiple instance learning network for whole slide image classification with self-supervised contrastive learning. In *Proceedings of the IEEE/CVF conference on computer vision and pattern recognition*, pages 14318–14328, 2021.
- [8] Zhuchen Shao, Hao Bian, Yang Chen, Yifeng Wang, Jian Zhang, Xiangyang Ji, et al. Transmil: Transformer based correlated multiple instance learning for whole slide image classification. *Advances in neural information processing systems*, 34:2136–2147, 2021.
- [9] Hongrun Zhang, Yanda Meng, Yitian Zhao, Yihong Qiao, Xiaoyun Yang, Sarah E Coupland, and Yalin Zheng. Dtf-dmil: Double-tier feature distillation multiple instance learning for histopathology whole slide image classification. In *Proceedings of the IEEE/CVF Conference on Computer Vision and Pattern Recognition*, pages 18802–18812, 2022.
- [10] Jinxi Xiang and Jun Zhang. Exploring low-rank property in multiple instance learning for whole slide image classification. In *The Eleventh International Conference on Learning Representations*, 2023.
- [11] Ming Y Lu, Richard J Chen, Jingwen Wang, Debora Dillon, and Faisal Mahmood. Semi-supervised histology classification using deep multiple instance learning and contrastive predictive coding. *arXiv preprint arXiv:1910.10825*, 2019.
- [12] Honglin Li, Chenglu Zhu, Yunlong Zhang, Yuxuan Sun, Zhongyi Shui, Wenwei Kuang, Sunyi Zheng, and Lin Yang. Task-specific fine-tuning via variational information bottleneck for weakly-supervised pathology whole slide image classification. *arXiv preprint arXiv:2303.08446*, 2023.
- [13] Ming Y Lu, Drew FK Williamson, Tiffany Y Chen, Richard J Chen, Matteo Barbieri, and Faisal Mahmood. Data-efficient and weakly supervised computational pathology on whole-slide images. *Nature biomedical engineering*, 5(6):555–570, 2021.
- [14] Yu Zhao, Fan Yang, Yuqi Fang, Hailing Liu, Niyun Zhou, Jun Zhang, Jiarui Sun, Sen Yang, Bjoern Menze, Xinjuan Fan, et al. Predicting lymph node metastasis using histopathological images based on multiple instance learning with deep graph convolution. In *Proceedings of the IEEE/CVF Conference on Computer Vision and Pattern Recognition*, pages 4837–4846, 2020.
- [15] Meyer Scetbon, Michael Elad, and Peyman Milanfar. Deep k-svd denoising. *IEEE Transactions on Image Processing*, 30:5944–5955, 2021.
- [16] Gabriele Campanella, Matthew G Hanna, Luke Geneslaw, Allen Miraflor, Vitor Werneck Krauss Silva, Klaus J Busam, Edi Brogi, Victor E Reuter, David S Klimstra, and Thomas J Fuchs. Clinical-grade computational pathology using weakly supervised deep learning on whole slide images. *Nature medicine*, 25(8):1301–1309, 2019.
- [17] Ji Feng and Zhi-Hua Zhou. Deep miml network. In *Proceedings of the AAAI conference on artificial intelligence*, volume 31, 2017.
- [18] Le Hou, Dimitris Samaras, Tahsin M Kurc, Yi Gao, James E Davis, and Joel H Saltz. Patch-based convolutional neural network for whole slide tissue image classification. In *Proceedings of the IEEE conference on computer vision and pattern recognition*, pages 2424–2433, 2016.
- [19] Marvin Lerousseau, Maria Vakalopoulou, Marion Classe, Julien Adam, Enzo Battistella, Alexandre Carré, Théo Estienne, Théophraste Henry, Eric Deutsch, and Nikos Paragios. Weakly supervised multiple instance learning histopathological tumor segmentation. In *Medical Image Computing and Computer Assisted Intervention—MICCAI 2020: 23rd International Conference, Lima, Peru, October 4–8, 2020, Proceedings, Part V 23*, pages 470–479. Springer, 2020.

- [20] Gang Xu, Zhigang Song, Zhuo Sun, Calvin Ku, Zhe Yang, Cancheng Liu, Shuhao Wang, Jianpeng Ma, and Wei Xu. Camel: A weakly supervised learning framework for histopathology image segmentation. In *Proceedings of the IEEE/CVF International Conference on computer vision*, pages 10682–10691, 2019.
- [21] Xinggang Wang, Yongluan Yan, Peng Tang, Xiang Bai, and Wenyu Liu. Revisiting multiple instance neural networks. *Pattern Recognition*, 74:15–24, 2018.
- [22] Yash Sharma, Aman Shrivastava, Lubaina Ehsan, Christopher A Moskaluk, Sana Syed, and Donald Brown. Cluster-to-conquer: A framework for end-to-end multi-instance learning for whole slide image classification. In *Medical Imaging with Deep Learning*, pages 682–698. PMLR, 2021.
- [23] Wentao Zhu, Qi Lou, Yeeleng Scott Vang, and Xiaohui Xie. Deep multi-instance networks with sparse label assignment for whole mammogram classification. In *International conference on medical image computing and computer-assisted intervention*, pages 603–611. Springer, 2017.
- [24] Michael Elad and Michal Aharon. Image denoising via sparse and redundant representations over learned dictionaries. *IEEE Transactions on Image processing*, 15(12):3736–3745, 2006.
- [25] Shuhang Gu, Wangmeng Zuo, Qi Xie, Deyu Meng, Xiangchu Feng, and Lei Zhang. Convolutional sparse coding for image super-resolution. In *Proceedings of the IEEE International Conference on Computer Vision*, pages 1823–1831, 2015.
- [26] Pan Xiao, Peijie Qiu, and Aristeidis Sotiras. Sc-vae: Sparse coding-based variational autoencoder. *arXiv preprint arXiv:2303.16666*, 2023.
- [27] Zhaowen Wang, Ding Liu, Jianchao Yang, Wei Han, and Thomas Huang. Deep networks for image super-resolution with sparse prior. In *Proceedings of the IEEE international conference on computer vision*, pages 370–378, 2015.
- [28] Mingyang Li, Pengyuan Zhai, Shengbang Tong, Xingjian Gao, Shao-Lun Huang, Zhihui Zhu, Chong You, Yi Ma, et al. Revisiting sparse convolutional model for visual recognition. *Advances in Neural Information Processing Systems*, 35:10492–10504, 2022.
- [29] Jian Zhang and Bernard Ghanem. Ista-net: Interpretable optimization-inspired deep network for image compressive sensing. In *Proceedings of the IEEE conference on computer vision and pattern recognition*, pages 1828–1837, 2018.
- [30] Jianchao Yang, John Wright, Thomas S Huang, and Yi Ma. Image super-resolution via sparse representation. *IEEE transactions on image processing*, 19(11):2861–2873, 2010.
- [31] Michal Aharon, Michael Elad, and Alfred Bruckstein. K-svd: An algorithm for designing overcomplete dictionaries for sparse representation. *IEEE Transactions on signal processing*, 54(11):4311–4322, 2006.
- [32] Ingrid Daubechies, Michel Defrise, and Christine De Mol. An iterative thresholding algorithm for linear inverse problems with a sparsity constraint. *Communications on Pure and Applied Mathematics: A Journal Issued by the Courant Institute of Mathematical Sciences*, 57(11):1413–1457, 2004.
- [33] Amir Beck and Marc Teboulle. A fast iterative shrinkage-thresholding algorithm for linear inverse problems. *SIAM journal on imaging sciences*, 2(1):183–202, 2009.
- [34] Stephen J Wright. Coordinate descent algorithms. *Mathematical programming*, 151(1):3–34, 2015.
- [35] Karol Gregor and Yann LeCun. Learning fast approximations of sparse coding. In *Proceedings of the 27th international conference on international conference on machine learning*, pages 399–406, 2010.
- [36] Abdul Qayyum, Aamir Saeed Malik, Mohamad Naufal, Mohamad Saad, Moona Mazher, Faris Abdullah, and Tuan Ab Rashid Bin Tuan Abdullah. Designing of overcomplete dictionaries based on dct and dwt. In *2015 IEEE Student Symposium in Biomedical Engineering & Sciences (ISSBES)*, pages 134–139. IEEE, 2015.
- [37] Babak Ehteshami Bejnordi, Mitko Veta, Paul Johannes Van Diest, Bram Van Ginneken, Nico Karssemeijer, Geert Litjens, Jeroen AWM Van Der Laak, Meyke Hermsen, Quirine F Manson, Maschenka Balkenhol, et al. Diagnostic assessment of deep learning algorithms for detection of lymph node metastases in women with breast cancer. *Jama*, 318(22):2199–2210, 2017.
- [38] Thomas G Dietterich, Richard H Lathrop, and Tomás Lozano-Pérez. Solving the multiple instance problem with axis-parallel rectangles. *Artificial intelligence*, 89(1-2):31–71, 1997.
- [39] Stuart Andrews, Ioannis Tsochantaridis, and Thomas Hofmann. Support vector machines for multiple-instance learning. *Advances in neural information processing systems*, 15, 2002.
- [40] Yann LeCun, Léon Bottou, Yoshua Bengio, and Patrick Haffner. Gradient-based learning applied to document recognition. *Proceedings of the IEEE*, 86(11):2278–2324, 1998.

- [41] Kaiming He, Xiangyu Zhang, Shaoqing Ren, and Jian Sun. Deep residual learning for image recognition. In *Proceedings of the IEEE conference on computer vision and pattern recognition*, pages 770–778, 2016.
- [42] Ting Chen, Simon Kornblith, Mohammad Norouzi, and Geoffrey Hinton. A simple framework for contrastive learning of visual representations. In *International conference on machine learning*, pages 1597–1607. PMLR, 2020.
- [43] Ming Tu, Jing Huang, Xiaodong He, and Bowen Zhou. Multiple instance learning with graph neural networks. *arXiv preprint arXiv:1906.04881*, 2019.
- [44] Yongluan Yan, Xinggang Wang, Xiaojie Guo, Jiemin Fang, Wenyu Liu, and Junzhou Huang. Deep multi-instance learning with dynamic pooling. In *Asian Conference on Machine Learning*, pages 662–677. PMLR, 2018.
- [45] Xiaolong Wang, Ross Girshick, Abhinav Gupta, and Kaiming He. Non-local neural networks. In *Proceedings of the IEEE conference on computer vision and pattern recognition*, pages 7794–7803, 2018.
- [46] Zhen Zhu, Mengde Xu, Song Bai, Tengpeng Huang, and Xiang Bai. Asymmetric non-local neural networks for semantic segmentation. In *Proceedings of the IEEE/CVF International Conference on Computer Vision*, pages 593–602, 2019.